MATERIALS PHYSICS AND MECHANICS RESEARCH ARTICLE

Submitted: April 30, 2026 **Revised: July 15, 2026** **Accepted: August 14, 2026**

Energy-absorbing metamaterials based on DNA helices

E.M. Farber ✉, A.V. Orlov, R. Ibrahiem, A.A. Popovich

Peter the Great St. Petersburg Polytechnic University, St. Petersburg, Russia

✉ d.farber2010@yandex.ru

ABSTRACT

The increasing demand for vehicle safety creates a need to develop of efficient protective systems with enhanced energy absorption performance. The results of the development and investigation of energy-absorbing metamaterials based on the DNA chain structure are presented. Computer simulation was carried out for preliminary determination of the metamaterial properties. Samples manufactured from Ti_6Al_4V alloy by the selective laser melting method were tested under quasi-static and dynamic compression. It was established that the specific energy absorption of the metamaterials under dynamic testing was 32.34 J/g, and under quasi-static testing, 14.22 J/g. The metamaterial withstands deformations exceeding 50 % without failure. The obtained results confirm the promising potential of the developed geometry for producing mechanical metamaterials with enhanced energy-absorbing characteristics.

KEYWORDS

metamaterial • energy absorption • DNA structure • selective laser melting

Funding. *This study was supported by the Ministry of Science and Higher Education of the Russian Federation (Agreement No. 075-15-2024-562).*

Citation: Farber EM, Orlov AV, Ibrahiem R, Popovich AA. Energy-absorbing metamaterials based on DNA helices. *Materials Physics and Mechanics*. 2026;54(4): 22–33.
http://dx.doi.org/10.18149/MPM.5442026_3

Introduction

To date, increasing attention and resources are being devoted to the development and design of protective systems for impact energy absorption [1]. Such systems can serve as energy-absorbing elements and structures necessary for reducing impact energy and protecting specific objects from detrimental effects [2,3]. Given the active development of transportation systems and the general trend toward increasing safety requirements, the integration of energy-absorbing elements into the structure of vehicles represents a promising engineering solution for minimizing damage in various emergencies [3,4]. As is known, during collisions or impacts, an energy absorption process occurs in which kinetic energy is converted into the internal potential energy of the system. Energy-absorbing elements are necessary to convert kinetic energy into potential energy through structural deformation [5]. Such energy conversion can be either irreversible (in the form of plastic deformation) or reversible (in the context of elastic deformation of materials). When designing energy-absorbing elements, the primary goal is generally the irreversible absorption of a significant portion of the kinetic energy generated upon impact, thereby minimizing the total damage to people and equipment [5–7].

To date, there are numerous examples of the application of energy-absorbing elements [8]: in the automotive industry, special crash boxes are developed and used in bumper structures and protective elements of electric vehicle battery packs [9,10], and

© E.M. Farber, A.V. Orlov, R. Ibrahiem, A.A. Popovich, 2026.
Publisher: Peter the Great St. Petersburg Polytechnic University
This is an open access article under the CC BY-NC 4.0 license (https://creativecommons.org/li-censes/by-nc/4.0/)

specialized crash barrier structures are developed [11]. In the aerospace industry, systems are being actively developed and implemented to protect crew and passengers during hard landings of helicopters and other aircraft [12]. Special attention is given to sports devices designed to protect individuals from potential injuries during sports activities [13,14].

Despite the relatively advanced level of development of existing energy-absorbing elements and structures, increasing safety requirements create a need for the development of qualitatively new elements that offer greater protective capabilities through improved energy absorption while maintaining low mass and structural stability. A promising direction in this regard is the potential use of metamaterials, specifically mechanical metamaterials. Mechanical metamaterials are artificially engineered materials with specific geometries of their unit cells—repeating units—capable of exhibiting certain unique properties, such as a negative Poisson's ratio or enhanced specific energy absorption [15–17]. A key feature of mechanical metamaterials is that their properties depend primarily on the geometry of their unit cells [18]. By altering the unit cell geometry, metamaterials with various properties can be obtained from the same base material [19].

One of the current trends in the design of metamaterials is the use of natural geometries [20]. This approach allows combining shapes and geometries refined over millions of years of evolution with modern design and manufacturing technologies for materials and structures, primarily additive manufacturing technologies, which enable the fabrication of products with geometries of varying complexity [20–23]. The use of nature-inspired design principles allows for the creation of metamaterials with high energy absorption performance based on geometries found in various living organisms [24–30]. A further development of this approach is the application of metamaterials to produce fully functional protective systems, for example, crash boxes filled with metamaterials having a specific structure, primarily based on honeycomb geometries [3,31,32]. Such approaches already yield systems with high levels of energy absorption. However, the need for enhanced safety conditions necessitates further developments in this direction. Foremost, there is a need for the development and investigation of new topologies of metamaterial unit cells capable of achieving higher values of energy absorption.

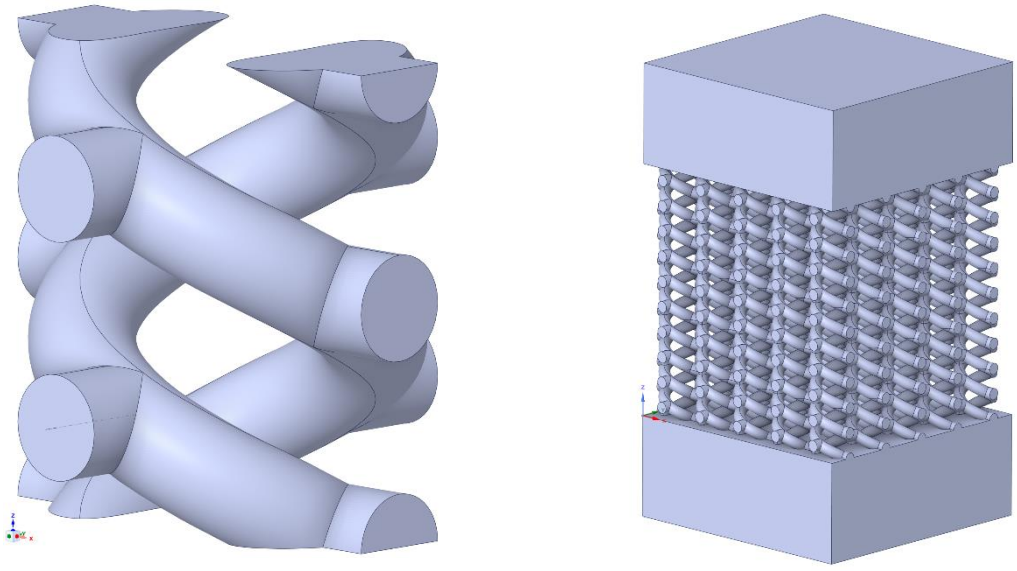
In view of the above-mentioned facts, the aim of this work is the design of mechanical metamaterials based on biomimetic geometry, their fabrication and testing to determine their mechanical properties and energy absorption parameters, with a subsequent assessment of the prospects for further application. In developing the initial geometry of the metamaterial unit cells, inspiration was initially drawn from the structure of the DNA helix, which was subsequently modified to obtain a stable and symmetric structure with a high level of performance. The metamaterial design process included numerical computer modeling to predetermine the full spectrum of its characteristics. The fabrication of metamaterial samples was carried out using the selective laser melting method from the Ti_6Al_4V alloy. The choice of this alloy is driven by the fact that it is one of the most widely used titanium alloys and is actively employed in additive technologies, including for the fabrication of mechanical metamaterials with geometries of varying complexity for various purposes. Testing included quasi-static and dynamic compression, followed by the determination of metamaterial properties and comparison with the

results of numerical computer modeling, consistent with the "simulation-experiment" approach. This approach allows for the validation and calibration of the computer model for subsequent use in designing full-scale products featuring the described geometry.

Materials and Methods

To determine the initial properties of the used Ti_6Al_4V alloy for numerical computer modeling, solid samples were fabricated with the following geometric parameters: d = 3 mm, h = 13 mm for samples intended for compression testing until fracture; d = 10 mm, h = 90 mm for determining the elastic modulus; d = 6 mm (gauge section), h = 63 mm for tensile testing; and d = 5.7 mm (gauge section), h = 53 mm for torsion testing. These samples, as well as the metamaterial samples, were fabricated from spherical powder of the Ti_6Al_4V alloy.

The samples were fabricated using the selective laser melting method on a 3DLAM Mini SLM system (by 3DLAM Company, Saint-Petersburg, Russia). The system is equipped with an IPG Photonics fiber laser. The build area is cylindrical, with a diameter of 90 mm and a height of 100 mm. The printing parameters were as follows: laser power of 150 W, scanning speed of 1200 mm/s, hatch distance of 0.12 mm, layer thickness of 0.03 mm, laser spot diameter of 0.08 mm. Fabrication was carried out in an argon atmosphere. The metamaterial samples were fabricated based on models with a porosity of 80 % and were oriented horizontally. After the fabrication of all samples, heat treatment was performed in a vacuum at a temperature of 1050 °C for 120 min, followed by furnace cooling.



(a) (b)

Fig. 1. Model of the unit cell (a) and the metamaterial sample (b) based on the DNA structure

The construction of the unit cell models and the metamaterial samples based on them, as well as the numerical computer modeling to determine their properties, was carried out using the ANSYS 2019 R2 SpaceClaim finite element analysis package. The unit cell dimensions are 2.5 mm along the three axes. The metamaterial samples consist of 5 cells along each of the three axes, totaling 125 unit cells. The final size of

the metamaterial sample model is 12.5 × 12.5 × 12.5 mm³. The model of the unit cell and the metamaterial sample is shown in Fig. 1. Additionally, base plates with dimensions of 12.5 × 12.5 × 5 mm³ were added to the top and bottom of the metamaterial sample for greater testing convenience.

For the constructed metamaterial models, the mechanical properties (elastic modulus (*E*), compressive yield strength, and compressive ultimate strength) were determined by numerical computer modeling of a compression experiment under static loading in both the elastic and plastic regions, using the finite element method within the ANSYS 2019 R2 SpaceClaim finite element analysis package. Elastic properties were determined by applying a 0.01 % strain to the upper face, while the lower face remained constrained with frictionless support. To capture the onset of failure and the plastic response, the displacement was increased to correspond to a 5 % strain.

To preliminarily determine the energy-absorbing characteristics of the metamaterials, an axial impact simulation was conducted using the ANSYS Explicit Dynamics finite element analysis package. For the alloy from which the metamaterials were manufactured, a multilinear plasticity model obtained from the results of mechanical tests was employed. Two parts were used for the simulation: the first was the metamaterial sample, and the second was the punch performing the impact. The finite element mesh consisted of 66,409 elements and 22,915 nodes. One end of the sample model was rigidly fixed, while the free end was subjected to impact by the punch at a velocity of 0.7 m/s. The punch velocity was specified both in the initial conditions and in the boundary conditions. In this way, conditions were created under which, from the very beginning of the simulation, the punch was already moving with an initial velocity and also continued its motion at a constant velocity. The simulation time was equal to 1.125e-2 s. During this time, the punch was displaced by 7.875 mm. Based on the simulation results, displacement and force values were obtained, which were used to calculate the energy absorption parameters.

Visual examination of the fabricated metamaterial samples before and after testing was performed using a TESCAN Mira 3 LMU scanning electron microscope (SEM) (TESCAN, Brno, Czech Republic) in secondary electron mode. Static compression tests until fracture and tensile tests were conducted using a Zwick/Roell Z100 universal testing machine. Torsion tests on solid samples, as well as dynamic compression tests (impact) until fracture of the metamaterial samples, were performed using a Gleeble 3800 system (Dynamic Systems Inc., Austin, TX, USA). During dynamic testing, the compression rate was 0.7 m/s.

The porosity of the fabricated metamaterial samples was calculated using the following equation:

$$P = (1 - \frac{\rho^*}{\rho_s}), \quad (1)$$

where ρ^* is the density of the metamaterial sample, and ρ_s is the density of the material from which the metamaterial sample is fabricated.

To evaluate the energy absorption of the metamaterial samples, several parameters were calculated. The baseline energy absorption (*EA*) was determined by mathematical integration of the stress-strain curve, which can be expressed by:

$$EA = \int_0^x F(x)dx. \quad (2)$$

The specific energy absorption (*SEA*) is used to evaluate the efficiency of energy absorption per unit mass of the structure under investigation and is calculated according to:

$$SEA = \frac{EA}{m}, \quad (3)$$

where m is the mass of the metamaterial sample.

Results and Discussion

Table 1 presents the list of properties of the Ti_6Al_4V alloy obtained from the tests on solid samples. These properties were used to perform numerical computer modeling to determine the properties of the metamaterials.

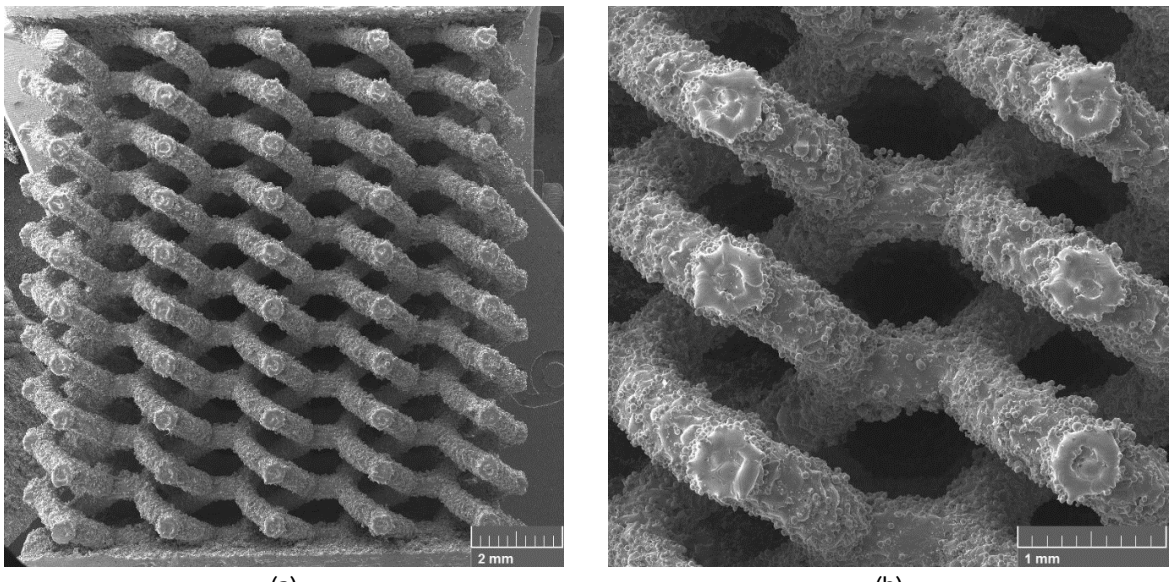
Table 1. Properties of the alloy

Parameters	**Value**
Density, ρ, kg/m^3	4387
Elastic modulus, *E*, GPa	155.78
Shear modulus, *G*, GPa	59.14
Poisson's ratio, ν	0.317

Based on the results of the numerical computer modeling, a list of properties of the metamaterials at 80% porosity was obtained, as presented in Table 2. In addition to the elastic modulus and yield strength, the energy absorption parameter was determined from the results of the impact test simulations, and the value of the specific energy absorption was calculated.

Table 2. Results of numerical computer modeling

Parameters	Values
Elastic modulus, GPa	0.238
Yield strength, MPa	7.4
Thickness of unit cell struts, μm	557
EA, J	42.92
SEA, J/g	25.25



(a) (b)

Fig. 2. SEM images of the fabricated metamaterial sample: (a) general view, (b) unit cells

Figure 2 presents SEM images of the fabricated metamaterial sample. Powder adhesion to the struts of the unit cells is observed. The porosity of the samples was 82.1 %. The average strut thickness was 494 μm.

Figure 3 presents the stress-strain curves obtained from the quasi-static compression tests of the metamaterial samples. High repeatability of the test results is observed. The samples deformed by 55–56 % (6.87–7.00 mm). The curves exhibit a pronounced deformation plateau without stress increase, during which gradual compression of the samples occurred. Further deformation was not performed due to complete compression and compaction of the unit cells of the metamaterial samples. The point of full compaction is observed on the curve (Fig. 3) in the deformation range from 50 to 55 %, where a gradual, followed by a sharp, increase in compressive stress occurs alongside a sharp decrease in the strain rate of the samples. Images of the metamaterial samples after quasi-static compression are shown in Fig. 4. The characteristics of the metamaterial samples obtained from the quasi-static compression tests are presented in Table 3.

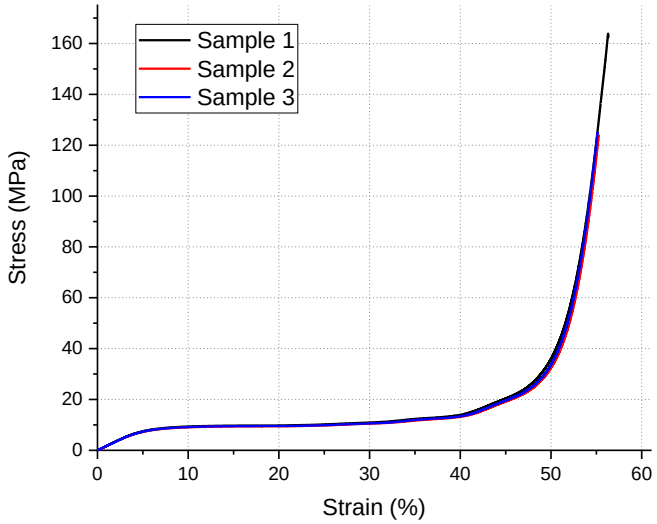
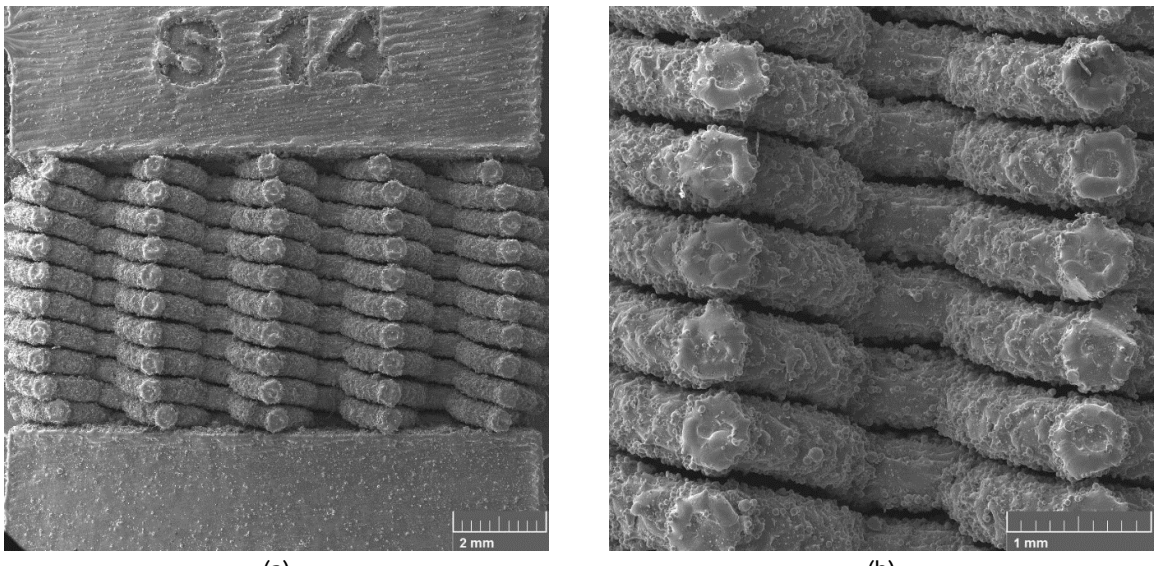


Fig. 3. Stress-strain curve of the metamaterial samples under quasi-static compression



(a) (b)

Fig. 4. Metamaterial sample after quasi-static compression: (a) general view, (b) unit cells

Figure 4 shows the results of compacting the metamaterial sample at the final stage of compression. The unit cells are deformed, and their struts almost touch each other, resembling a spring compressed to its solid height. At the same time, no cracks or failure of the unit cell elements are observed. A slight lateral expansion of the sample can be noted.

As can be seen from Table 3, the obtained results for the samples exhibit minimal deviations and a high degree of repeatability. The average conditional elastic modulus was 0.17 GPa, and the average conditional yield strength was 6.2 MPa. The conditional ultimate strength was not determined, as no actual fracture of the sample occurred during the compaction process. A comparison with the results obtained from numerical computer modeling is presented in Table 4. Deviations from the simulated values are observed for all presented parameters. Notably, the deviations in the conditional elastic modulus and yield strength are on the lower side. The deviation in the elastic modulus was 28.57 %, while the deviation in yield strength was slightly lower at 16.22 %. The overall reason for these deviations lies in the change in sample porosity. The porosity of the fabricated samples turned out to be 2.1 % more than that of the original model, which logically led to a reduction in mechanical properties. Furthermore, the potential presence of micropores or other defects in the struts of the metamaterials could also have contributed to the decrease in mechanical properties. It should be noted that despite the presence of deviations, the numerical computer modeling yielded values close to the experimental ones. The maximum deviation was less than 30 %. It can be confidently stated that the presented "simulation-experiment" methodology is effective and allows for successful preliminary evaluation of the properties of designed metamaterials. At the same time, further refinement of the methodology is necessary to improve the accuracy of the results.

Table 3. Properties of the metamaterial samples obtained from the compression test results

	Conditional elastic modulus, GPa	**Conditional yield strength, MPa**	**Max. deformation, %**	**Stress at max. strain, MPa**
Sample 1	0.173	6.39	56.33	163.88
Sample 2	0.167	6.10	55.27	123.78
Sample 3	0.170	6.10	55.13	124.76
Average	0.170	6.20	-	-
Standard deviation	0.003	0.16	-	-

Table 4. Comparison of simulation results and experimental studies

	Simulation	**Experiment**	**Deviation, %**
Porosity, %	80	82.1	2.1
Strut thickness, μm	557	493	11.49
Conditional elastic modulus, GPa	0.238	0.170	28.57
Conditional yield strength, MPa	7.4	6.2	16.22

Figure 5 presents the load-displacement curves obtained from the dynamic compression tests. The energy absorption and specific energy absorption values of the samples, calculated from the results of the dynamic and quasi-static compression tests, are presented in Table 5.

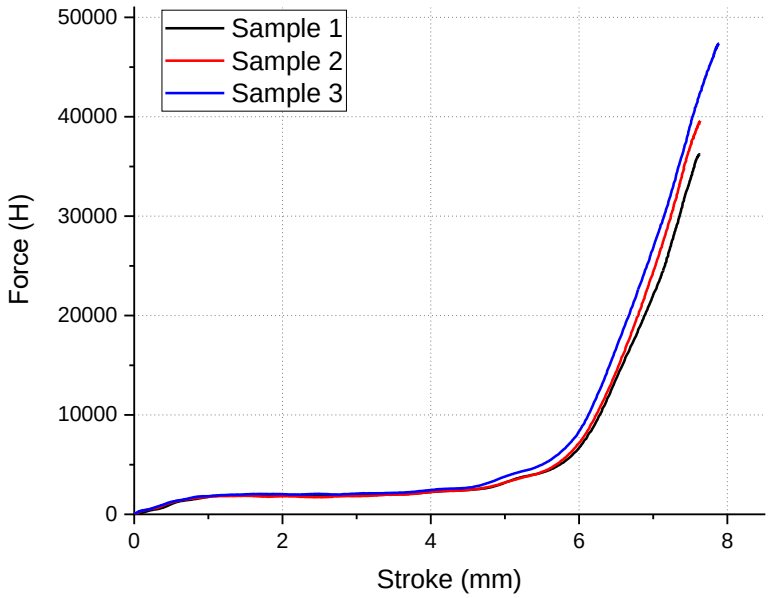


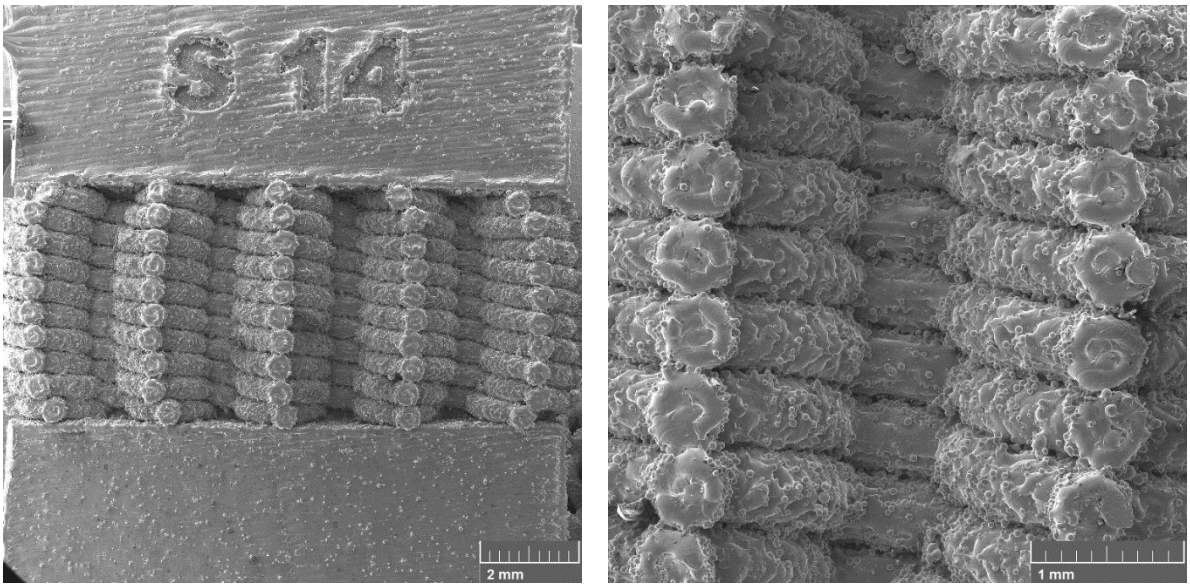
Fig. 5. Stroke-force curves of the crosshead for the metamaterial samples under dynamic compression

Table 5. Energy absorption characteristics of the metamaterial samples.

Test		***EA*, J**	***SEA*, J/g**
Dynamic compression	Sample 1	45.90	30.40
	Sample 2	47.65	31.35
	Sample 3	52.90	35.27
	Average	48.82	32.34
	Standard deviation	3.64	2.58
Quasi-static compression	Sample 1	14.57	9.40
	Sample 2	13.94	9.23
	Sample 3	14.15	9.31
	Average	14.22	9.31
	Standard deviation	0.32	0.08

As can be seen from Fig. 5, the deformation process of the samples, characterized in this case by crosshead displacement, is similar to the deformation observed during quasi-static compression. Initially, the samples begin to deform and compact, as indicated by the shallow region of the curve, followed by a further increase in compressive force at the stage of completed sample compaction. Moreover, no actual fracture of the samples occurs. As with quasi-static compression, a high level of repeatability of the results is observed. Figure 6 shows the sample after dynamic testing. As in the quasi-static tests, in this case compaction of the sample occurred. All cells are compressed and contact each other with their struts. Likewise, no fractured cells or cracks are observed.

From Table 5, it can be seen that the specific energy absorption under dynamic testing averaged 32.34 J/g, which is more than three times higher than that under quasi-static testing. At the same time, the deviations in the results under dynamic compression are larger than those under quasi-static compression. The highest specific energy absorption value under dynamic compression testing was obtained for sample 3, reaching 35.27 J/g. Under quasi-static testing, the highest specific energy absorption was 9.4 J/g, with an average value of 9.31 J/g.



(a) (b)

Fig. 6. Metamaterial sample after dynamic compression: (a) general view, (b) unit cells

To compare the simulation results with the experimental data for dynamic compression, the data are summarized in Table 6. In contrast to the quasi-static compression results, in this case the simulation results were lower than the experimental ones. The energy absorption value from the experiment was 12 % higher than that predicted by the simulation results. The specific energy absorption value obtained experimentally was also higher than the simulated values, by nearly 22 %. The observed discrepancies between the simulated and experimental results may be attributed to insufficient modeling accuracy, which does not allow for taking into account all influencing factors. Such factors may include a reduction in the porosity of the experimental samples, which can affect the final mass and influence the calculation of *SEA* values, possible errors in data recording by the testing machine, as well as inaccuracies in the experimental determination of the absorbed energy value. Nevertheless, it should be noted that the results demonstrate a satisfactory level of accuracy, with deviations not exceeding 22 %.

Table 6. Comparison of simulation results and experimental studies

	Simulation	**Experiment**	**Deviation, %**
EA, J	42.92	48.82	12.08
SEA, J/g	25.25	32.34	21.92

The obtained data on the energy absorption of the developed metamaterials should be compared with the results reported in open literature sources. The specific energy absorption of the metamaterials under dynamic testing was 32.34 J/g. When recalculated taking into account the volume of the working section of the sample, the volumetric specific energy absorption averaged 24.45 MJ/m^3 at a density of 787 kg/m^3. This value of volumetric specific energy absorption falls within the range of values typical for titanium alloy metamaterials presented in reference [21]. Under quasi-static testing, the specific energy absorption was 14.22 J/g. The obtained results are several times higher than, for

example, those in reference [27], which presented TPMS-type geometry metamaterials made of Ti_6Al_4V alloy with a specific energy absorption of less than 3 J/g. At the same time, reference [33] presented Ti_6Al_4V alloy metamaterials based on TPMS geometries with a porosity gradient, exhibiting volumetric specific energy absorption in the range of 31 to 54 MJ/m^3, which is somewhat higher than the values obtained in our work. Also worth noting is reference [16], where metamaterials with a pomelo peel-inspired geometry, also fabricated from Ti_6Al_4V alloy, demonstrated a specific energy absorption of 44.16 J/g.

Taken together, the presented data indicate the overall representativeness of our results. The developed geometry exhibits energy absorption parameters close to the best results published in open sources. Consequently, further research is necessary to improve its energy absorption characteristics. One possible approach to enhancing energy absorption may be a slight reduction in the porosity of the metamaterial sample to achieve optimal energy absorption performance.

Conclusions

In this work, metamaterial samples with a geometry designed based on the DNA helix were fabricated using the SLM method and investigated. The mechanical characteristics of the metamaterial samples were obtained, and the energy absorption properties were determined under both quasi-static and dynamic compression testing. As a result, it was established that the presented "simulation-experiment" methodology is effective. Even taking into account deviations in the porosity of the fabricated metamaterial samples, the deviations in the final properties between the model and the experiment did not exceed 30 %. The obtained metamaterial samples do not possess high mechanical characteristics; however, due to their high ductility—which is a feature of the geometry—they withstand deformations of more than 50 % without any fracture, even upon reaching the compaction stage under quasi-static compression.

The energy absorption of the obtained metamaterial samples generally corresponds to the level of energy absorption of structures with various geometries fabricated from titanium alloys. The specific energy absorption of the metamaterials under dynamic testing was 32.34 J/g, while under quasi-static testing it was 14.22 J/g. Under dynamic testing, the samples also do not fracture but merely compact.

The obtained results generally indicate the promise of using the presented geometry for producing mechanical metamaterials with enhanced energy absorption characteristics. Research in this direction should be continued, including with regard to modifying the presented unit cell geometry to achieve higher energy absorption values, as well as designing energy-absorbing systems and devices based on the data already obtained.

CRediT authorship contribution statement

Eduard M. Farber: conceptualization, investigation, writing – review & editing; **Aleksei V. Orlov**: investigation; writing – review & editing; **Raihana Ibrahiem**: writing – original draft; **Anatoliy A. Popovich**: data curation, supervision.

Conflict of interest

The authors declare that they have no conflict of interest.

References

1. Guo C, Mao J, Xie M. Study on energy absorption characteristics of aluminum foam composite anti - collision rod. *J Brazilian Soc Mech Sci Eng.* 2022;44(7): 1–14.
2. Khoa ND, Bohara RP, Ghazlan A, Thai T, Ngo T. Novel hierarchical bioinspired cellular structures with enhanced energy absorption under uniaxial compression. *Aerosp Sci Technol.* 2024;147: 108995.
3. Fachrudin AR, Choiron MA, Purnowidodo A, Irawan YS. Crashworthiness simulation dataset of re-entrant crash box with combined in-plane and out-of-plane filling structure. *Data Br.* 2025;61: 111820.
4. Kondakov I, Chernov A, Guseva N, Levchenkov M. Protective elements for lattice composite fuselage structures against low-velocity impacts. *Aerosp Syst.* 2022;5(1): 1–9.
5. Chahardoli S, Nia AA, Asadi M. Parametric investigation of the mechanical behavior of expanding-folding absorbers and their implementation in sandwich panels core. *Thin-Walled Struct.* 2019;137: 53–66.
6. Isaac CW, Ezekwem C. A review of the crashworthiness performance of energy absorbing composite structure within the context of materials, manufacturing and maintenance for sustainability. *Compos Struct.* 2021;257: 113081.
7. Sepahvand Y, Morshedsolouk F, Moazemi Goudarzi A. Experimental and numerical study of energy absorption in bio- inspired scutoid cellular structures. *Materials Physics and Mechanics.* 2025;53(6): 63–81.
8. Siddique SH, Hazell PJ, Wang H, Escobedo JP, Ameri AAH. Lessons from nature: 3D printed bio-inspired porous structures for impact energy absorption – A review. *Addit Manuf.* 2022;58: 103051.
9. Gürses D. Enhanced crash performance of multi-cell crash box for electric vehicle battery pack design. *Mater Test.* 2025;67(10): 1707–1714.
10. Wang H, Wang Z, Du X, Wang N. Design of a New Energy Absorbing Box with Honeycomb Structure for Vehicles and Research on Vehicle Crashworthiness. *Iran J Sci Technol - Trans Mech Eng.* 2025;49(4): 1813–1832.
11. Wang X, Li Z, Hao H, Chen W. Experimental study on energy absorption performance of kirigami-modified honeycomb module for crash cushion. *Eng Struct.* 2026;353: 122227.
12. Yang X, Ma J, Wen D, Yang J. Progress in Aerospace Sciences Crashworthy design and energy absorption mechanisms for helicopter structures: A systematic literature review. *Prog Aerosp Sci.* 2020;114: 100618.
13. Wang X, Li Y, Yu H, Habibi M. Parametric Optimization of 3D-Printed Reentrant Metamaterials for Energy Absorption in Protective Sport Devices. *Adv Eng Mater.* 2026;28(3): 1–12.
14. Jiang Y, Yao J, Yang S, Habibi M, Norouzi M. Bio-Inspired Mechanical Metamaterial Architectures: Parametric Optimization of Novel 3D-Printed Structures for Sports Equipment. *Int J Struct Stab Dyn.* 2026;2750222: 1–23.
15. Farber E, Orlov A, Popovich A. Design and characterization of additively manufactured energy-absorbing mechanical metamaterials with bioinspired geometries. *Mater Sci Addit Manuf.* 2026;5(2): 025360082.
16. Zhang Z, Song B, Fan J, Wang X, Wei S, Fang R, et al. Design and 3D Printing of Graded Bionic Metamaterial Inspired by Pomelo Peel for High Energy Absorption. *Chinese J Mech Eng Addit Manuf Front.* 2023;2(1): 100068.
17. Maslov LB, Borovkov AI, Nezhinskaya LS, Zhmaylo MA, Tarasenko FD. Strength characteristics of additively manufactured meta-biomaterials made of titanium alloy under cyclic loading. *Materials Physics and Mechanics.* 2025;53(5): 50–73.
18. Jin H, Espinosa HD. Mechanical Metamaterials Fabricated From Self-Assembly: A Perspective. *J Appl Mech.* 2024;91(4): 1–7.
19. Jiao P, Mueller J, Raney JR, Zheng X, Alavi AH. Mechanical metamaterials and beyond. *Nat Commun.* 2023;14(1): 6004.
20. Zhou Q, Xu Z, Cui Y, Wang K, Wang B. Out-of-plane compression and energy absorption performance of twisted auxetic honeycomb tubes. *Int J Eng Sci.* 2026;220: 104435.
21. Bernard AR, ElSayed MSA. Design, Manufacturing, and Analysis of Periodic Three-Dimensional Cellular Materials for Energy Absorption Applications: A Critical Review. *Materials (Basel).* 2024;17(10): 2181.
22. Xia P, Liu Q, Fu H, Yu Y, Wang L, Wang Q, et al. Mechanical properties and energy absorption of 3D printed double-layered helix honeycomb under in-plane compression. *Compos Struct.* 2023;315: 116982.
23. Isaac CW, Duddeck F. Current trends in additively manufactured (3D printed) energy absorbing structures for crashworthiness application – a review. *Virtual Phys Prototyp.* 2022;17(4): 1058–1101.

24. Yin X, Cui H, Hu H, Xu H, Yang T. Design and mechanical characterization of novel triply periodic minimal surface-based lattice structures with high strength and energy absorption. *Compos Struct.* 2026;382: 120062.
25. Wang P, Guo J, Yuan Y, Li C, Wang Y, Guang M, Yan J, Liu W, Sun Z. Bio-inspired vertex-offset lattice metamaterials with enhanced stress stability and energy absorption. *Thin-Walled Struct.* 2025;210: 113060.
26. Zhu Y, Chen Z, Zhu Y, Gresil M, Tang Y. Bio-inspired perturbated hierarchical mechanical metamaterial for energy absorption. *Int J Mech Sci.* 2025;307: 110847.
27. Guo X, Li X, Wang E, Fuh JYH, Lu WF, Zhai W. Bioinspired hierarchical diamond triply periodic minimal surface lattices with high energy absorption and damage tolerance. *Addit Manuf.* 2023;76: 103792.
28. Han D, Lin K, Luo Q, Li P, Ni X, Wang P, et al. Experimental and numerical investigations of bio-inspired hollow re-entrant auxetic metamaterials manufactured using laser powder bed fusion. *J Mater Res Technol.* 2025;39: 4898–4912.
29. Zhiguang Z, Zhenlin C, Xiao H, Chaozhi L, Yang S, Zhaowei D, et al. Radial Buckling-Harnessed Auxetic Effect for Enhanced Energy Absorption in Snowflake-Perforated Honeycomb Metamaterials. *Adv Eng Mater.* 2026;28(1): 1–11.
30. Wu S, Fu T. Design and Energy Absorption Performance of a Framed Diamond-Star Honeycomb Structure with Dual-Plateau Response. *Appl Compos Mater.* 2026;33(1): 10.
31. Bader ST, Hamzah MN, Atiyah QA. Numerical Investigation of Energy Absorption in Graded Honeycomb-Filled Composite Crash Box Structures. *Int J Automot Technol.* 2026;27(2): 755–765.
32. Nian Y, Ni YQ, Avcar M, Yue R, Zhou K. Novel negative-zero-positive Poisson's ratio graded mechanical metamaterials for enhanced energy absorption: Performance investigation and design optimization. *Eng Struct.* 2025;343: 121092.
33. Zhao M, Zhang DZ, Liu F, Li Z, Ma Z, Ren Z. Mechanical and energy absorption characteristics of additively manufactured functionally graded sheet lattice structures with minimal surfaces. *Int J Mech Sci.* 2020;167: 105262.